


RESEARCH LETTER

Open Access



# Discovery of a conical feature in Halmahera waters, Indonesia: traces of a late-stage hydrothermal activity

Gabriella Alodia<sup>1\*</sup> , Nurhidayat<sup>2</sup>, Dyan P. Sobarudin<sup>2</sup>, Dian Adrianto<sup>2</sup>, Angga Dwinovantyo<sup>3</sup>, Steven Solikin<sup>4</sup>, Mustafa Hanafi<sup>5</sup>, Astyka Pamumpuni<sup>6</sup>, Idham A. Kurniawan<sup>7</sup>, Poerbandono<sup>1</sup>, Chris M. Green<sup>8</sup> and Andrew M. McCaig<sup>8</sup>

## Abstract

An expedition to confirm the presence of underwater hazards was carried out in Halmahera waters, Indonesia, to the west of Halmahera Island from August to September 2021. The expedition carried out a multibeam survey, surface-towed magnetic survey, and seafloor sampling. A ~615-m-tall conical feature with traces of hydrothermal activity was discovered. The feature is bounded on the southeastern (SE) side by a series of normal faults at the peak, with possible dextral strike-slip faults traced west of the feature. The feature displays the potential presence of volcanic rocks based on the observed contrasting magnetic anomaly signature of down to –100 nT, which at the magnetic equator corresponds to the presence of highly magnetised material. Four 2.5-D magnetic models were built to test various scenarios on the subsurface structure of the feature, mainly focusing on the presence of volcanic rocks at different epochs and a possible presence of serpentinitisation. X-ray diffraction (XRD) of the silt and clay sediments sampled confirms traces of late-stage hydrothermal activity, indicated by a high percentage of quartz (53.87%), followed by calcite (34.56%), kaolinite (6.54%), and illite minerals (5.04%). Non-carbonate materials are yet to be found in the sampled sand and gravel sediments, which mainly consist of shell and coral fragments. The discovery of the conical feature, now termed the Yudo Sagoro Hill, provides new information on the structure and activities on the seafloor of Halmahera waters.

**Keywords** Multibeam bathymetry, Magnetic anomaly, X-ray diffraction (XRD), Serpentinite seamount, Hydrothermal activity, 2.5-D magnetic modelling

\*Correspondence:

Gabriella Alodia  
gabriella.alodia@itb.ac.id

<sup>1</sup> Hydrography Research Group, Faculty of Earth Sciences and Technology, Institut Teknologi Bandung (ITB), Bandung, Indonesia

<sup>2</sup> Hydro-Oceanographic Centre, Indonesian Navy, Jakarta Utara, Indonesia

<sup>3</sup> Research Centre for Oceanography, The National Research and Innovation Agency (BRIN), Jakarta Utara, Indonesia

<sup>4</sup> Department of Marine Science and Technology, Faculty of Fisheries and Marine Sciences, IPB University, Bogor, Indonesia

<sup>5</sup> Research Centre for Geological Resources, The National Research and Innovation Agency (BRIN), Jakarta Pusat, Indonesia

<sup>6</sup> Applied Geology Research Group, Faculty of Earth Sciences and Technology, Institut Teknologi Bandung (ITB), Bandung, Indonesia

<sup>7</sup> Petrology, Volcanology, and Geochemistry Research Group, Faculty of Earth Sciences and Technology, Institut Teknologi Bandung (ITB), Bandung, Indonesia

<sup>8</sup> School of Earth and Environment, University of Leeds, Leeds, UK

## Introduction

Through Indonesian notice to mariners (*"Berita Pelayar Indonesia"* or BPI), underwater hazards in the form of rapid underwater movement (BPI no. 11/152; Pushidrosal 1955) and boiling waters (BPI no. 26/206; Pushidrosal 1959) were reported in Halmahera waters. The rapid underwater movement is described to be situated between 01° 00' N, 129° 00' W and 00° 18' N, 129° 54' W (Fig. 1c), with a diameter of 15 nautical miles. The boiling water is described to be located approximately 12 nautical miles east of Jiew Island (00° 43' 0.4 N, 129° 07' 0.9 W). As the region is located at the edge of Indonesian waters, an initiative was undertaken to obtain a physical description of the reported hazard to update the nautical charts used for the safety of navigation at sea. The initiative, the Jalacitra I-2021 expedition 'Aurora', was carried out in three legs from 13 August to 21 September 2021 aboard the KRI Spica 934 of the Indonesian Navy Hydro-Oceanographic Centre or 'Pushidrosal'. During the expedition, a conical underwater feature was discovered within the area of the underwater hazards described. This paper discusses the physical descriptions of the newly discovered feature and its possible relation to the underlying magmatic and tectonic activities in this little-known region.

## Geological setting

### The East Halmahera-Waigeo ophiolite terrane (EHWOT)

Part of the crust in the Halmahera region has been described as the East Halmahera-Waigeo ophiolite terrane (Charlton et al. 1991; Milsom et al. 1996a). The ophiolite complex has no continental basement and consists of a complete sequence of dismembered ophiolitic rocks, with a potential exception of a sheeted dyke complex (Hall et al. 1988a, b; Ballantyne 1992). Crustal thicknesses within the complex are on the order of 21–27 km based solely on gravity modelling (Milsom et al. 1996a) and 12–20 km in parts where seismic reflection data are available (Milsom et al. 1996b). These numbers are consistent with the findings of Chen et al. (1992) and Su et al. (1994), which state that the crust in the EHWOT region is much thicker than the typical 6-km-thick oceanic

crust. Milsom et al. (1996a) interpret that thickening might occur in Layer 2, where an increase of extrusive and high-level intrusive rocks occurs, patterns found in oceanic islands (Mutter and Mutter 1993). The EHWOT can be traced to the eastern Philippine terrane, making it part of the larger Philippine Sea Plate (Hall, 1988). Sampled rocks in the ophiolite complex are also reported to be similar to rocks dredged from the Mariana Trench (Bloomer 1983; Ballantyne 1992). Dimalanta et al. (2020) reported that the volcanic rocks in the EHWOT include both mid-ocean ridge basalt, back-arc basin basalt, and island arc tholeiite. Therefore, the EHWOT is believed to be formed in a supra-subduction zone environment (Ballantyne 1991, 1992), where ophiolites formed above a subduction zone (e.g., Wakabayashi et al. 2010).

### Tectonic boundaries traced from vertical gravity gradient (VGG)

The tectonic boundaries of the western Pacific can be described by computing the VGG of a global free air gravity anomaly data set (Fig. 1a) (Sandwell et al. 2014; topex.ucsd.edu/cgi-bin/get\_data.cgi) and the bathymetry GEBCO\_2022 (GEBCO, 2022; gebco.net). The VGG calculation was carried out using the *gravfft* function of the GMT software version 5.4.5 (Wessel et al. 2013). The traced tectonic boundaries are shown in Fig. 1b. The feature names are adapted from Milsom et al. (1992), Milsom et al. (1996b), Lee and Kim (2004), and the NCEI Trackline Geophysical Data Viewer (ncei.noaa.gov/maps/geophysics).

As shown in Fig. 1b, the Halmahera waters are situated in a complex interaction zone between the Eurasian, Pacific, Philippine Sea, and Caroline plates (e.g., Hall 1987; Milsom et al. 1992). In the northwest, the Philippine Sea Plate convergence is accommodated through the Philippine Trench, whereas the convergence of the Pacific Plate is accommodated through the New Guinea Trench further east of the area (e.g., Hamilton 1979; Nichols et al. 1990). No link has been found between these two convergent boundaries (Milsom et al. 1996b). Hall et al. (1988a, b) reported that the Philippine Trench does not extend south of about 2° N. The Manokwari trough and the New Guinea Trench can be traced southeast of

(See figure on next page.)

**Fig. 1** Tectonic setting of the western Pacific and study area. **a** Vertical gravity gradient (VGG) of the western Pacific. **b** Tectonic boundaries traced from discontinuities/lineaments visible from the VGG. **c** Tectonic setting of the study area. Background bathymetry is taken from GEBCO\_2022 (GEBCO, 2022; gebco.net). Earthquake data are downloaded from the ISC-GEM Catalogue (Di Giacomo et al. 2018). The seismogenic region is mostly characterised by strike-slip motion depicted by the dark blue 'beach balls' (Ekström et al. 2012), apart from a thrust fault (dark red 'beach ball') west of the newly traced East Halmahera Trough. Magenta square: Estimated location of underwater hazards in the form of rapid underwater movement (BPI no. 11/152; Pushidrosal 1955) and boiling waters (BPI no. 26/206; Pushidrosal 1959), as presented in the text. Red square: A 'seismic gap' area. Dashed grey line: The East Halmahera-Waigeo ophiolite terrane (EHWOT) boundary, after Milsom et al. (1996a). Black rectangle: East Halmahera Trough traced from the VGG, shown in **d**. The VGG colour scale is similar to **a**



whose origin remains controversial (Lee and Kim 2004). The trough has been linked to the late Palau-Kyushu Ridge, east and west Mariana Ridges, as well as the active Izu-Ogasawara (Bonin)-Mariana, Yap, and Palau trenches due to their correlating pattern (Cardwell et al. 1980; Hutchison 1986). A divergent boundary indicates an upwelling of the lithospheric mantle at the Ayu Trough, induced by the small motion differences between the Philippine Sea and Caroline plates (Hall 2002).

### Tectonic setting based on the ISC-GEM earthquake catalogue

The tectonic setting of the study area can be described by the seismicity of the region based on the published ISC-GEM Global Instrumental Earthquake Catalogue (Di Giacomo et al. 2018; [isc.ac.uk/iscgem](http://isc.ac.uk/iscgem); Fig. 1c). Prominent tectonic activity is observed in the Philippine Trench, where deep-seated earthquakes (up to 250 km) occur over the subducting slab. Shallow earthquakes of < 50 km depth are observed in the vicinity of the newly traced East Halmahera Trough (Fig. 1c and 1d). Further east of the trench, little to no seismic activity was found in the vicinity of the Manokwari Trough. Several GCMT ‘beach balls’ (Ekström et al. 2012) show that most of the earthquakes in the study area record strike-slip motion (dark blue ‘beach balls’ in Fig. 1a), except one thrust fault motion recorded west of the newly traced East Halmahera Trough (dark red ‘beach ball’ in Fig. 1a). These moment tensors reflect the generally dextral strike-slip motion across the Halmahera Sea, transferring the convergence between the Philippine Sea and Eurasia plates (McCaffrey 1982; Nichols et al. 1990).

As the reported underwater hazard is located in a ‘seismic gap’ between the seismicity of the Philippine Trench, East Halmahera Trough, and the scattered shallow seismicity of the Manokwari Trough, we pose questions on the possible source of any hydrothermal activities in this region.

### Field data acquisition: multibeam bathymetry, surface-towed magnetic survey, and seafloor sampling

Field data were acquired through the Jalacitra I-2021 ‘Aurora’ expedition. The expedition was divided into three legs, arranged according to logistical strategy. The details of each leg are shown in Table 1.

A multibeam bathymetry survey was carried out to obtain seafloor depths and identify the morphology of the underwater hazard/conical feature. Seafloor classification was performed by analysing the backscatter of the instrument. The shipboard multibeam bathymetry survey was carried out using the Kongsberg EM302 multibeam echosounder (MBES) with a standard frequency of 30 kHz. The survey was carried out with a line spacing of approximately 0.3 to 1.5 km (wider spacing in deeper areas), resulting in a total survey length of around 3000 km (Fig. 2b). The effects of tides were removed in multibeam processes using instantaneous water levels observed by the Veripos LD8 GNSS-tide. The results are gridded into a 10-m cell size using Caris HIPS and SIPS 9.0 based on the 5- to 7-m general resolution obtained during the survey.

A magnetic survey was carried out to obtain the magnetic signature of the conical feature using a Geometrics G-882 marine magnetometer. The line spacing of the magnetic survey ranges from 300 to 600 m, following the line spacing of the concurrent multibeam survey over the feature. The survey vessel, KRI Spica 934, is a dedicated survey vessel built primarily with aluminium with an overall length of 60.1 m. As the vessel is not made of a highly magnetic material (e.g., iron), the magnetometer was towed ~ 100 m behind the vessel instead of following the standard three times vessel length. Due to time constraints, only five magnetic survey lines (each approximately 3 km long; Fig. 3a) were obtained over the volcanic feature.

Seafloor sampling was carried out using a standard Van Veen grab sampler (e.g., Smith and McIntyre 1954) with a 15 × 15 cm size. Due to the time constraints, sampling was only carried out at a point close to the peak of the

**Table 1** Scope of work and dates of each survey leg

Survey leg	Scope of work	Dates	Survey duration (days)	Data volume
Leg 1	Multibeam bathymetry survey, surface-towed magnetic survey over the object of interest	13 to 23 Aug 2021	9	Bathymetry: ~ 1000 km Magnetic: ~ 15 km
Leg 2	Multibeam bathymetry survey (continued from Leg 1), grab sampling	28 Aug to 7 Sept 2021	9	Bathymetry: ~ 1000 km Grab sampling: 4 trials, 1 successful
Leg 3	Multibeam bathymetry survey (continued from Leg 2)	12 to 21 Sept 2021	8	Bathymetry: ~ 1000 km

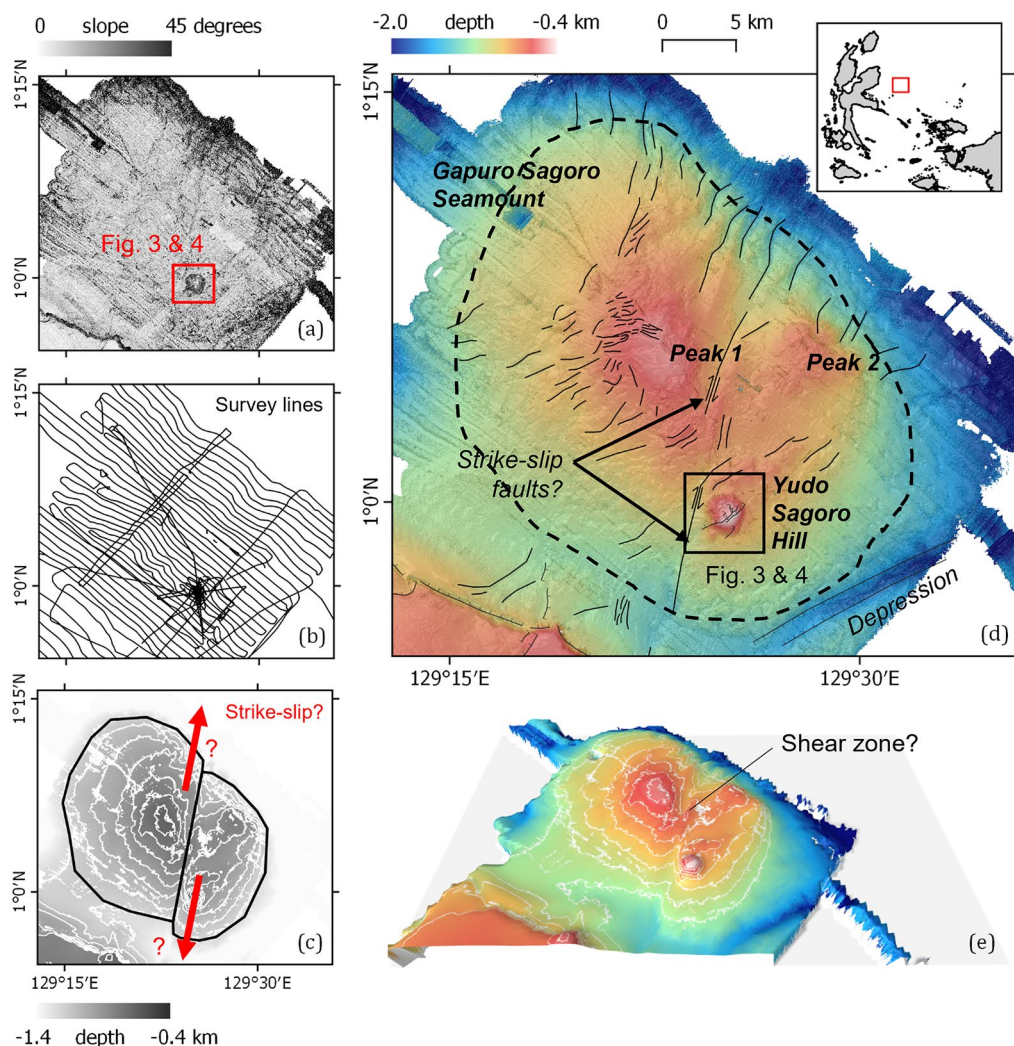


**Fig. 2** Bathymetric map of the Gapuro Sagoro Seamount, the northern part of the survey area. **a** Bathymetric slope. The red square indicates a sub-feature with a steeper slope than its surrounding. **b** Multibeam bathymetry survey lines. **c** Interpreted motion based on perceived morphology. White lines: 100-m contour lines. **d** Bathymetric map of the study area with perceived lineaments and sub-features. Dashed lines: the Gapuro Sagoro Seamount. Based on the perceived motion in **c**, supported by the moment tensors in the vicinity of the feature (see Fig. 1), two dextral strike-slip faults were traced west of the Yudo Sagoro Hill. **e** 3-D view of the feature, highlighting a possible shear zone in the middle of the feature. The toponyms of ‘Gapuro Sagoro Seamount’ and ‘Yudo Sagoro Hill’ have been documented in the GEBCO Undersea Feature Names ([gebco.net/data\\_and\\_products/undersea\\_feature\\_names/](http://gebco.net/data_and_products/undersea_feature_names/))

volcanic feature (lon: 129.4235° E; lat:0.9913° N; depth: 411 m) based on the guidance from the multibeam backscatter analysis, which will be detailed in section **Seabed sediment classification and seafloor samples**. Of four sampling trials, only one was successful. As the survey vessel is relatively lightweight, rock sampling through dredging was not carried out for safety reasons.

**Seafloor morphology**

The depth of the study area ranges from 393 to around 2400 m (Fig. 2d). The 31-km-wide Gapuro Sagoro Seamount was detected in the northern part of the study

area, with three peaks separated by two faults striking almost N–S, interpreted from the obtained multibeam bathymetry. We interpret these two faults as dextral strike-slip faults based on perceived movements from the obtained morphology (Fig. 2c) and a perceived shear zone in the middle of the seamount (Fig. 2e). One of the peaks is indicated to have a much steeper slope than the other two (Fig. 2a), hence described as the conical feature, the Yudo Sagoro Hill (Pushidrosal 2022). The conical feature is around 3.6 km wide and 615 m high, undetected in the most recent GEBCO\_2022 bathymetry nor documented in published studies. The shallowest area of the feature

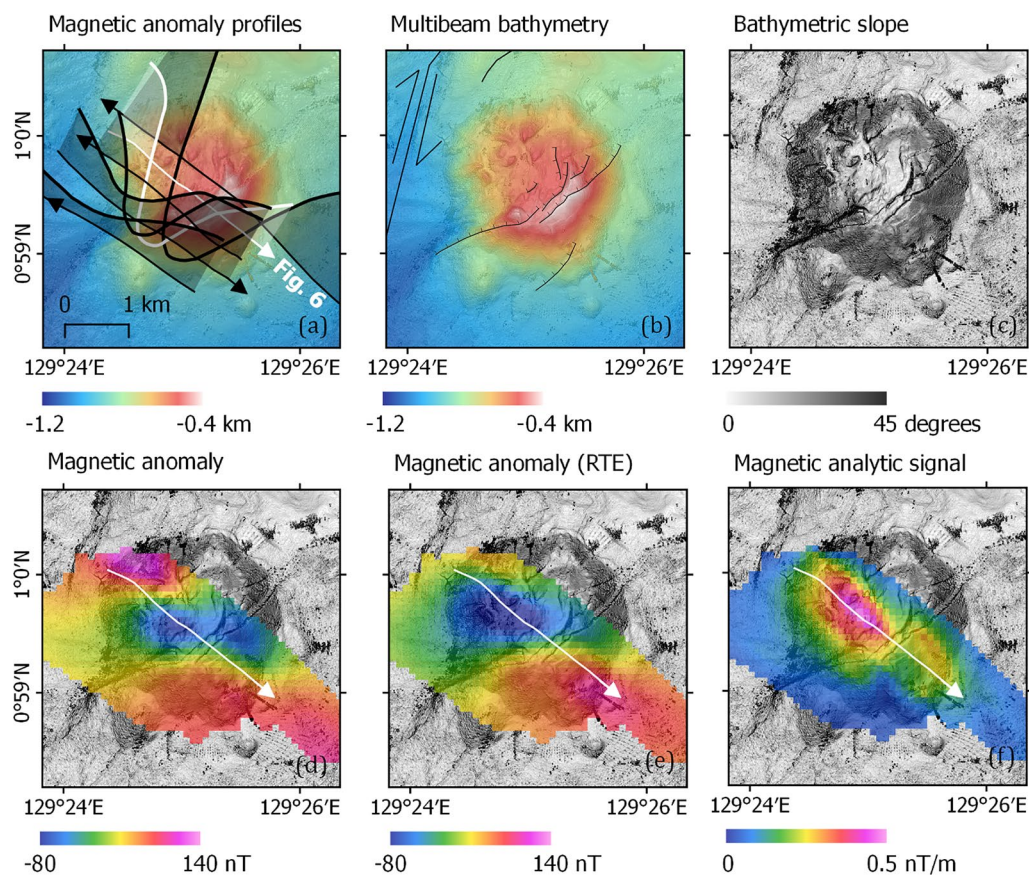


**Fig. 3** The conical feature: Yudo Sagoro Hill. **a** Multibeam bathymetry overlaid with magnetic profiles/wiggles. Black wiggles: surveyed magnetic profile in each survey line. White wiggles: surveyed magnetic profile in the middle of the feature, used in the 2.5-D magnetic modelling in Fig. 6. White arrow: survey direction of the centre line. **b** Multibeam bathymetry with interpreted faults. **c** Bathymetric slope. **d** Gridded magnetic anomaly. **e** RTE of the magnetic anomaly. **f** Analytic signal of the RTE magnetic anomaly

is around 393 m below the sea surface and the deepest is around 1008 m below the sea surface (Fig. 3a and b). The feature is characterised by slopes as steep as 45°, with parallel normal faults at the peak dipping ~60° NW (Fig. 3b and c). East of the Gapuro Sagoro Seamount is a NE–SW striking depression with the deepest mapped area of 1980 m (Fig. 2d).

#### Seafloor magnetic anomaly

The magnetic anomaly of the conical feature is obtained by performing standard magnetic data processing, including levelling and transformation from the observed total magnetic intensity to magnetic anomalies based on the IGRF2020 model (Alken et al. 2021). The magnetic survey track and the resulting magnetic anomaly wiggles at each line are illustrated in Fig. 3a. Magnetic anomaly data were gridded at a resolution of 100 m (Fig. 3d) using the adjustable tension continuous curvature splines method through the *blockmean* and *surface* functions of the software GMT 5.4.5 (Wessel

et al. 2013). Extrapolated data outside of the survey lines were omitted using a mask created from a *near-neighbor* interpolation of the obtained data set with a search radius of 600 m, following the 300–600 m survey line spacing over the feature.

A reduction-to-equator (RTE) operator (e.g., Aina 1986) was applied to the gridded data set through the GRAV-MAG Suite (Castro et al. 2018; [github.com/fcastro25/GravMagSuite](https://github.com/fcastro25/GravMagSuite); Fig. 3e). The RTE operator was applied instead of the reduction-to-pole (RTP) operator, as the RTP methods are unstable and less useful at low magnetic latitudes (e.g., Swain 2000). From the RTE magnetic anomalies, an analytic signal operator is applied (Nabighian 1972; Salem et al. 2002) to locate the source of the observed magnetic anomalies. The resulting grid shows two loci of high magnetic anomaly signatures: one was located close to the peak of the feature extending NW and another was located SE of the higher anomaly (Fig. 3f).

### Seabed sediment classification and seafloor samples

Acoustic backscatter from the multibeam was used to classify the types of sediments on the feature. Seabed materials with high hardness levels, e.g., rocks and gravels, are depicted with higher backscatter values than softer materials, e.g., clay and silt (Wienberg and Bartholomä 2005). A rough seabed is also depicted with a higher backscatter value than a smoother seabed. The backscattering strengths in dB are then classified into seabed sediment types with specified ranges. In this study, we processed the extracted acoustic backscatter using Sediment Analysis Tools of the software Caris 9.0.

Backscatter intensity values over the conical feature range between  $-38$  and  $-12$  dB (Fig. 4a). To obtain accurate seafloor classification, the backscatter grid is

analysed using the Geocoder engine (Fonseca and Calder 2005). The engine has an algorithm to apply radiometric and geometric corrections to the multibeam backscatter data to produce backscatter mosaics from the raw multibeam data. The backscatter data correction includes slope correction for time-varying gain, transmit and receive gain, beam pattern, and angular-varying gain. The characteristics of seafloor sediments were estimated based on backscatter mosaic information using the angular range analysis method (Fonseca and Mayer 2007). The filtered backscatter mosaic data are those within the near-range incidence angle ( $0^\circ$  to  $25^\circ$ ) due to the high confidence level (Fonseca et al. 2009). Data outside the near-range incidence angle were filtered out (Fig. 4b).

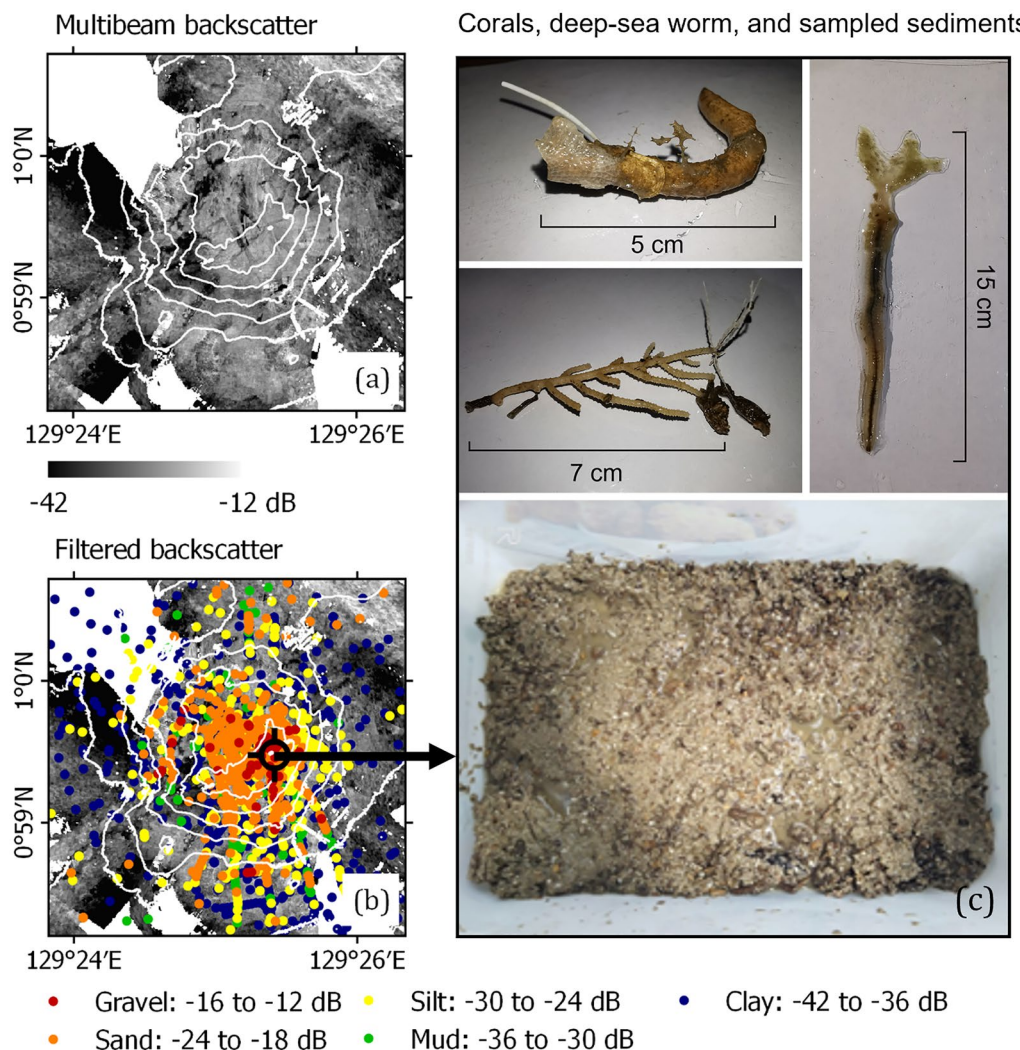


**Fig. 4** Multibeam backscatter and sampled materials from one successful trial. **a** Multibeam backscatter of the conical feature. White lines: 100-m contours. **b** Filtered multibeam backscatter showing seabed classification. An area with the highest number of high-decibel backscatters was chosen for seafloor sampling. **c** Seafloor biota and sediments sampled from the peak of Yudo Sagoro Hill

Guided by the sediment classification of Kloser and Keith (2013), the seabed sediment is classified into clay (−42 to −36 dB), mud (−36 to −30 dB), silt (−30 to −24 dB), sand (−24 to −18 dB), and gravel/harder substrate (−16 to −12 dB). The base of the feature is dominated by clay. The area close to the peak is dominated by sand, topped with a significant area of gravel/harder substrate. Sediment sampling is carried out in an area with the highest number of high-decibel backscatter (lon: 129.4235° E; lat: 0.9913° N; depth: 411 m) to validate the classification, as indicated in Fig. 4b. From the sampling station, multi-granular sediments were recovered (Fig. 4c), dominated by sands (78.37%), followed by gravel (15.35%), clay (5.47%), and silt (0.57%), as detailed in Table 2. Microscopic observation of the sand and gravel reveals that they were composed of shell and coral fragments. The silt and clay sediments were brought to a laboratory as explained in section **Laboratory treatment: X-ray diffraction (XRD) analysis** for further investigation. In addition, fresh cold-water corals and a living deep-sea worm with a length of ~15 cm were also recovered from the sampling station (Fig. 4c). The cold-water corals are part of the family *Isididae*, while the sea worm is part of the class *Polychaeta* tube worm.

## 2.5-D magnetic forward modelling

2.5-D magnetic forward modelling was carried out using the software GEOMODEL 2.00 (Cooper 1998) to interpret the subsurface structure of the conical feature. A 2.5-D model was chosen as opposed to the 2-D approach because, in a 2.5-D model, an end correction is applied to the bodies in the cross-section to account for a limited extent outside of the plane (e.g., in Prezzi et al. 2005; Noutchogwe et al. 2010). In this study, the model was limited to a depth of 2 km based on the limited length of the survey line (~3 km). The constraints used were the depths of the seafloor and the field magnetic anomaly. The cross-section runs 127° east of

north, with a magnetic inclination of −13.91° and a magnetic declination of 0.33° based on the IGRF2020 model (Alken et al. 2021). As the feature is situated near the magnetic equator, highly magnetised bodies were depicted with an extremely low magnetic signature as opposed to high (e.g., Breiner 1973). Volcanic rocks, e.g., basalt, are the most magnetic compared to the other types of rocks. Therefore, in all models, at least one volcanic body was introduced based on the significant magnetic anomaly value observed in the survey line (down to −100 nT) with the basement and surrounding rocks being highly altered volcanic crust with minimum magnetic susceptibility. Sedimentary covers are modelled at the flanks of the feature to fit the field magnetic anomaly data better, as the model is constrained by the depth profile of the feature. The resulting models are shown in Fig. 5.

The first model (Fig. 5a) depicts a volcanic body with a magnetic susceptibility of 0.0055 cgs. The second model (Fig. 5b) introduces a slightly higher magnetic susceptibility to the volcanic body ( $S=0.006$  cgs) and an intrusive body with a magnetic susceptibility of 0.0025 cgs. The intrusive body depicts a possible presence of altered materials in addition to the volcanic body. Other possible scenarios would be to introduce volcanic bodies with remanent magnetisation. In the third model (Fig. 5c), a volcanic body with remanent magnetisation with the same intensity as the magnetisation of the previous volcanic bodies and an inclination of 2° is introduced. The inclination is calculated from a general magnetic dipole equation of a geocentric axial dipole (GAD) hypothesis (e.g., Veikkolainen et al. 2014):

$$\tan(I) = 2\tan(\lambda), \quad (1)$$

where  $I$  is the inclination and  $\lambda$  is the paleo-latitude. According to paleomagnetic studies of Hall et al. (1995a) and Hall et al. (1995b), the Halmahera region has been close to the equator for the last 25 Ma. The Yudo Sagoro Hill is currently located at around 1° latitude. Inserting this value into Eq. 1, 2° is a reasonable magnetisation direction for recently (<0.78 Ma) magnetised material. This assumption would require the magnetisation to be mostly remanent, but that has certainly been observed in basalts (e.g., Dietze et al. 2011). The final model (Fig. 5d) incorporates the possibility of a volcanic body close to the surface with a maximum depth of 0.9 km, underlain by two volcanic bodies with remanent magnetisation with an inclination of 2°. The bigger remanent body has 1.35 times the magnetic intensity of the other magnetised bodies. In all models, the susceptibility of the highly altered volcanic crust is set to 0.0005 cgs. No susceptibility value was assigned to the sedimentary covers.

**Table 2** Classification of sediments sampled from the Yudo Sagoro Hill

Sediment type	Grain size (mm)	Weight (g)	Quantity (%)
Gravel	2.000–4.000	15.35	15.51
Sand	1.000–2.000	26.53	26.81
	0.500–1.000	12.97	13.10
	0.250–0.500	17.82	18.01
	0.125–0.250	18.26	18.45
	0.063–0.125	1.98	2.00
Silt	0.004–0.064	0.57	0.58
Clay	<0.004	5.47	5.53



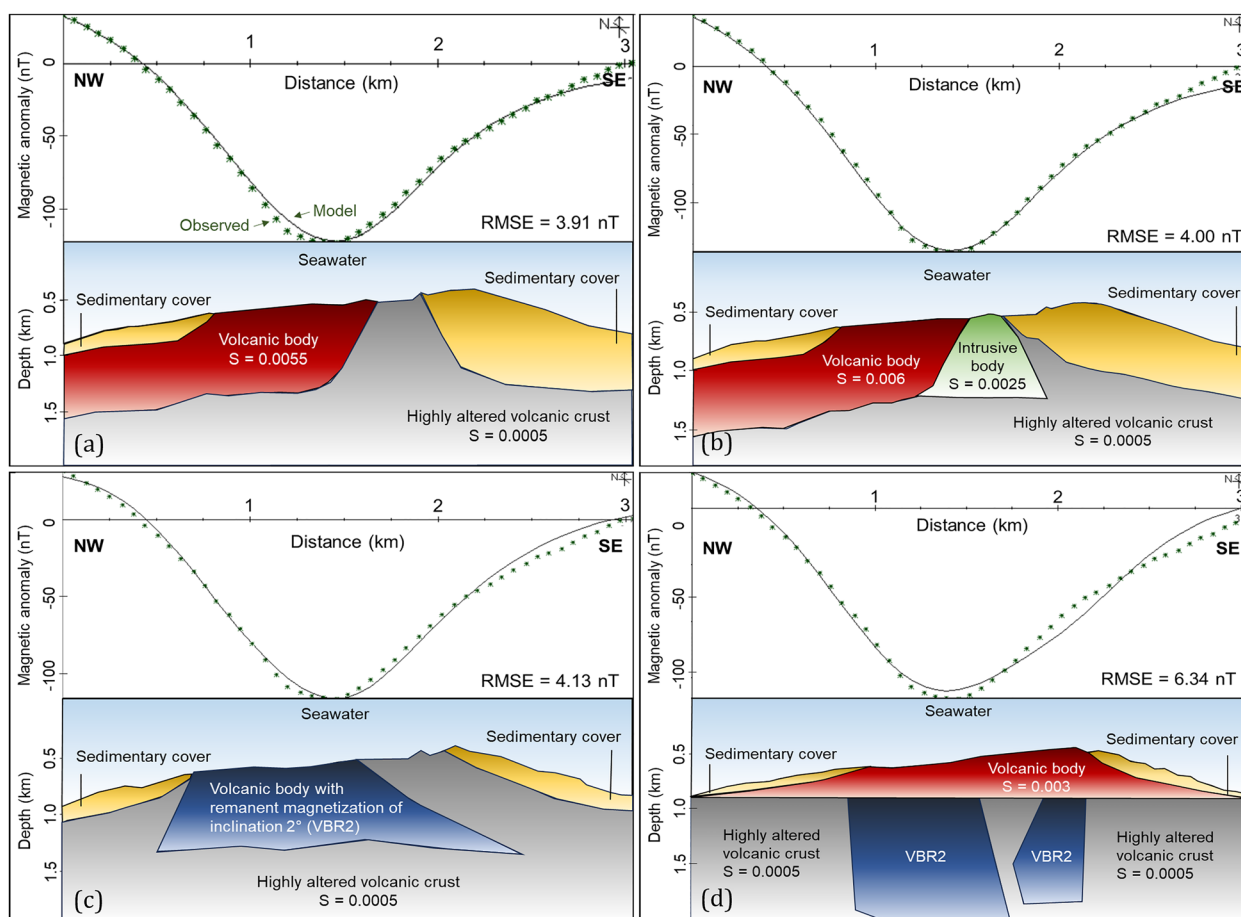


**Fig. 5** Subsurface structure based on 2.5-D magnetic forward modelling. Stars: observed magnetic anomaly. Solid line: modelled magnetic anomaly. Profile bearing:  $127^\circ$ . Inclination:  $-13.91^\circ$ . Declination:  $0.33^\circ$ . The root mean square errors (RMSE) of each model are displayed. **a** A volcanic body ( $S=0.0055$  cgs) was introduced into the model, with a highly altered volcanic crust ( $S=0.0005$  cgs) below and sedimentary cover with no magnetisation on both sides (NW and SE). **b** An intrusive body ( $S=0.0025$  cgs) was introduced into the model (**a**) to represent the possible presence of altered/serpentinised materials. The volcanic body was set at 0.006 cgs. **c** A volcanic body with remanent magnetisation of  $2^\circ$  inclination (VBR2) was introduced to model a more typical field direction in the present magnetic epoch in the equator. **d** Two VBR2 bodies underlie a volcanic body of 0.003 cgs susceptibility, which dominates the surface of the feature. The bigger underlying volcanic body has 1.35 times the magnetic intensity of the other magnetised bodies

### Laboratory treatment: X-ray diffraction (XRD) analysis

An XRD test using copper (Cu) radiation was carried out on the silt and clay sediments (grain size  $<0.064$  mm) sampled from the Yudo Sagoro Hill to discover any trace of serpentinisation, volcanism, or hydrothermal activities. The XRD test was carried out using the clay-orientated preparation method of USGS (pubs.usgs.gov/of/2001/of01-041/html/docs/methods.htm). Laboratory tests were not carried out on the sand and gravel samples as they are dominated by shell and coral fragments based on microscopic observations. The XRD pattern (Fig. 5) shows traces of illite, kaolinite, quartz, and calcite minerals. The percentage of each mineral is shown in Table 3. A

detailed description and interpretation of the XRD pattern will be discussed in section [Present situation: a late-stage hydrothermal activity](#).

### Discussion

#### Yudo Sagoro Hill: a hydrothermal reactivation of a subdued structure

Based on the guidance of BPI no. 11/152 (Pushidrosal 1955) and BPI no. 26/206 (Pushidrosal 1959), the Gapuro Sagoro Seamount was discovered in Halmahera waters. Compared to the coordinates in both documents, the feature is located in the northern part of the 'BPI area' (Fig. 1c). Morphologically, the Gapuro Sagoro Seamount can be interpreted as a subdued structure based

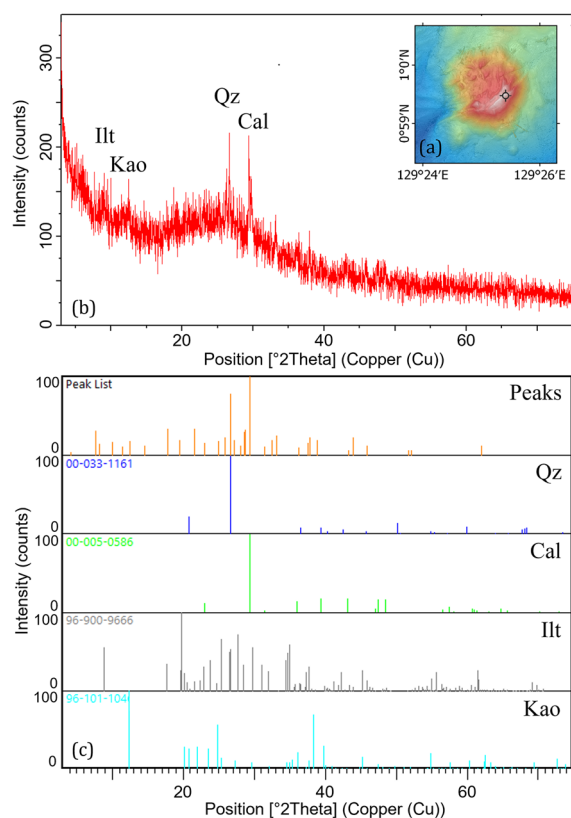


**Fig. 6** XRD patterns of clay and silt sediment samples on the Yudo Sagoro Hill using copper (Cu) radiation, with reference to crystallography.net/cod. **a** Sampling station (lon: 129.4235° E; lat: 0.9913° N; depth: 411 m). **b** Overall XRD diffractogram showing peaks of illite (Ill), kaolinite (Kao), quartz (Qz), and calcite (Cal). The peaks of each indicated mineral are shown in **c**

**Table 3** XRD results of the silt and clay sediments sampled from the Yudo Sagoro Hill

Mineral	2-Theta (°)	d-spacing (Å)	Area (cts*2Th)	Semi-quantity (%)
Ill	8.2185	10.74955	1.14	5.04
Kao	11.4731	7.70648	1.48	6.54
Qz	26.6452	3.34282	12.19	53.87
Cal	29.3986	3.03571	7.82	34.56

on its generally gentle slopes. Two N–S bearing faults were traced in the middle of the seamount. Based on the perceived geometry and morphology (Fig. 2c), we interpret these two faults as dextral strike-slip faults formed by an apparent dextral shear motion on the seamount (Fig. 2e). Although the age of the volcanic activity and faults are still unknown, it is plausible that these faults might be responsible for the drawdown of the surficial

water, triggering the activation of a hydrothermal system at Yudo Sagoro Hill. As the shearing motion seems to ‘divide’ the seamount, we interpret that the strike-slip faults were formed after the main volcanic activities have been suppressed.

The seamount consists of three peaks. One of them, the Yudo Sagoro Hill, depicts a more recent volcanic activity, characterised by steeper slopes, which forms a noticeable conical shape (Fig. 2a and d). Compared to Peak 1 and Peak 2, a much steeper slope is observed on the Yudo Sagoro Hill. This contrasting morphology led us to interpret that this peak might result from a reactivation of the subdued Gapuro Sagoro Seamount.

In addition to its morphology, the Yudo Sagoro Hill is interpreted to contain some form of volcanic rocks based on the magnetic anomaly signatures obtained over the feature, ranging from around  $-100$  to  $140$  nT. Near the magnetic equator, highly magnetised materials are depicted by a low magnetic signature (e.g., Breiner 1973). After applying RTE and analytic signal operators to the gridded magnetic anomaly data set, the result shows that the anomaly is centred in an area that morphologically resembles a mudflow (Fig. 3e and f).

To further investigate the possible structure of the Yudo Sagoro Hill, 2.5-D magnetic modelling was carried out with four different scenarios. The first model (Fig. 5a) shows the presence of a volcanic body, which corresponds to highly magnetised volcanic deposits running in the middle of the structure, flowing NW. The boundary between the volcanic body and the highly altered volcanic crust might represent the tectonic boundary, which in the bathymetry represented the NW-dipping series of normal faults.

In the second model (Fig. 5b), we introduced an intrusive body with a lower susceptibility value in addition to the volcanic body. The lower susceptibility could correspond to the alteration of the same volcanic material that could occur due to the drawing down of seawater through the strike-slip faults. Seawater might interact with deep-seated magmatic rocks and emerge to form a hydrothermal vent and leave traces of altered volcanic rocks. This interpretation is strengthened by the sampled biota associated with a deep-sea coral reef ecosystem that could only survive in a favourable living condition, e.g., in an existing hydrothermal vent (e.g., Lutz and Kennish 1993).

Another interpretation of the intrusive body would be debris flows of serpentinite materials flowing from the top of the feature, as mostly found in the Marianas (e.g., Fryer 1996, 2012; Wheat et al. 2020) based on the similarity between the rocks sampled at the EHWOT and the Marianas (e.g., Ballantyne et al., 1992). Ophiolitic rocks were found in many places in the EHWOT. For instance, on

Waigeo, the Lamlam Formation of probable Late Eocene age consists of ultrabasic sandstones, siltstones, and sedimentary breccias (Charlton et al. 1991). On East Halmahera, the Paniti Formation of Middle-Upper Eocene also consists of conglomerates, sandstones, siltstones, mudstones, coals, and limestones with mostly ophiolitic non-carbonate debris (Hall et al., 1991). As the study area is located between the Halmahera and Waigeo islands, serpentinite sediments and ophiolitic basement could be present below or within Yudo Sagoro Hill.

The third model (Fig. 5c) introduced another scenario, where several volcanic bodies (VBR2 in Fig. 5c and d) were assigned a remanent magnetisation more typical of the field direction in the present magnetic epoch in the equator (2° inclination based on Eq. 1). This scenario investigates the subsurface structure of the volcanic feature if the volcanic activity started around 0.78 Ma or younger. In the fourth model (Fig. 5d), we incorporate bodies with remanent magnetisation with a volcanic body of lower magnetic susceptibility, suggesting alteration after the body interacts with seawater. However, the low magnetic inclination might also indicate Neogene rocks as old as 15 Ma, as opposed to younger rocks (e.g., Hall et al. 1995a, b). This scenario can also be considered if the magnetic signature is interpreted to be formed by hydrothermal alteration of an older feature.

To assess these models, a closer inspection of the sampled sediments was carried out. Through microscopic investigations, we found that most of the sand and gravel sediments consist of foraminifera shell and coral fragments with no signs of non-carbonate debris, which do not distinguish between the different models. However, the result of the XRD analysis confirms the presence of a hydrothermal alteration process, which will be detailed in section **Present situation: a late-stage hydrothermal activity**. We interpret the finding as a 'late-stage' activity, as traces of hydrothermal alteration were only indicated in the finest grained sediment. Earlier stage alteration should be more easily indicated in the coarser fragments, i.e. the gravels.

#### **Present situation: a late-stage hydrothermal activity**

As discussed in section **Laboratory treatment: X-ray diffraction (XRD) analysis**, the XRD pattern shows traces of quartz (53.87%), calcite (34.56%), kaolinite (6.54%), and illite (5.04%). These minerals are the result of an epithermal alteration process with a relatively low temperature and a moderately low fluid pH (Corbett and Leach 1997). The high percentage of quartz and calcite might imply that the alteration results from the mixing of cool, descending, low pH sulphate and/or CO<sub>2</sub>-rich surficial fluids with hot silica-saturated deep hydrothermal fluids (Leach et al. 1985; Simmons and Christensen 1994;

Reyes 1991). If such deep hydrothermal fluids exist, it would suggest that the Gapuro Sagoro Seamount was part of a formerly active hydrothermal system that has been subdued, consistent with what is perceived from its bathymetry.

The hydrothermal system might be reactivated by drawing surficial fluids into the fractures of the two dextral strike-slip faults in the middle of the subdued seamount. This interpretation correlates well with the presence of kaolinite and illite minerals, representing a phyllic/argillic alteration zone adjacent to a major structure (Corbett and Leach 1997). However, the absence of higher temperature products such as sericite and pyrophyllite implies that the clay minerals were formed by an argillic alteration, ruling out the possibility of a phyllic alteration. Continuous drawdown of acidic fluids through the fractures could result in higher mineral deposition, which would develop an impermeable cap on the system, lowering the activity of the hydrothermal system (Lawless et al. 1983). Another interpretation is that calcite minerals might be formed from depositional materials from undersea biota, namely from corals and foraminifera shells. This interpretation is consistent with our sea-floor samples, in which the sampled sands and gravels are composed of shells and coral fragments. Additionally, the obtained living biota depicted favourable living conditions at the sampling site.

The remaining question would be the source of magnetisation in this late-stage hydrothermal activity and the most probable subsurface structure. Argillic alteration is often associated with volcanic activity, as acidic gases released from the activity could lower the pH of the fluids drawn down to the fractures (e.g., Taran and Kalacheva 2020). This type of alteration can overprint earlier phyllic alteration, depositing pyrite, local chlorite, and carbonite in addition to kaolinite and illite (Corbett 2008). Although mainly described to be weakly paramagnetic (e.g., Schneider et al. 2004), ferromagnetic tendencies have been noted in pyrite (e.g., Waters et al. 2007), which might be responsible for the intense magnetisation indicated over the feature. Remanent magnetisation through serpentinisation of exposed peridotite (e.g., Oufi et al. 2002) could also occur considering the lower susceptibility body modelled in Fig. 5b. On the other hand, the two later models (Fig. 5c and d) representing 'young volcanism' implies that magnetisation might come from fresh volcanic rocks, such as andesites that contain abundant magnetite and titanomagnetite. Such rocks are common in Halmahera and are Paleogene, Neogene, and Quaternary (Hall et al. 1988b).

Regarding the most probable subsurface structure, the model in Fig. 5b correlates best with the interpretation that hydrothermal reactivation was triggered by the

drawing of surficial waters to the fractures of the strike-slip faults on the Gapuro Sagoro Seamount. In this model, an 'intrusive' body with a lower susceptibility value than the 'volcanic' body was introduced. The presence of this body allows interpretations of either alteration of volcanic material or magnetisation of exposed peridotite to occur on the feature, while the other models consider only volcanic materials on the structure. However, this interpretation comes with the caveat that the silt and clay samples obtained from the feature were merely 6.04 g from one location of the whole feature. A more thorough seafloor sampling at different locations, possibly with different instruments (e.g., box corer, dredger, etc.) is required to distinguish between the proposed models. Seafloor inspection through a camera-equipped remotely operated vehicle (ROV) operation will also be useful to find indications of chimneys and massive sulphide deposits (MSD).

### Conclusions

This study has conducted a pioneering survey by carrying out a multibeam bathymetry survey, backscatter analysis, magnetic survey, and seafloor sediment sampling on a previously unknown feature east of Halmahera Island, Indonesia. The survey was motivated by an indication of underwater hazards reported in the Indonesian notice to mariners, or BPI, in 1955 (BPI no. 11/152; Pushidrosal 1955) and 1959 (BPI no. 26/206; Pushidrosal 1959). The survey found a 31-km-wide subdued structure with three peaks at the northern part of the BPI area, that is, the Gapuro Sagoro Seamount. Among the three peaks, one is indicated to have a much steeper slope than the other, that is, the Yudo Sagoro Hill. Based on morphology, physical characteristics, and geochemistry tests of sediment samples through XRD, we infer that this peak is part of a reactivation of a subdued volcanic system previously unknown in the EHWOT region.

Yudo Sagoro Hill shows a striking magnetic anomaly of  $-100$  nT about its centre, which in an area near the magnetic equator implies the presence of a highly magnetic material. A multibeam backscatter analysis indicated a sand-dominated peak, which further guided the seafloor sampling processes. The sampling confirms the domination of the sands at the peak (78.37%), with a minor presence of gravel (15.51%) and mud materials (0.58% silt, 5.53% clay). Furthermore, living deep-water biota were also obtained from the successful sampling process, showing favourable living conditions at a depth of 411 m.

Four scenarios of subsurface structures were introduced through a 2.5-D magnetic forward modelling. Each model consists of a highly altered volcanic crust as the basement and surrounding rocks, with: (1) a 0.0055 cgs volcanic body lying NW from the centre of the

feature; (2) a similar volcanic body with 0.006 cgs with a 0.0025 cgs intrusive body at the centre of the feature; (3) a remanently magnetised volcanic body with magnetisation inclination of  $2^\circ$  calculated from the paleo-latitude of the feature, and; (4) a 0.003 cgs volcanic body underlain by two remanently magnetised volcanic bodies with varying magnetisation intensity and magnetisation inclination of  $2^\circ$ .

Despite the lack of geological data to prove the validity of these models, the clay minerals identified from the XRD analysis confirm the presence of hydrothermal activities in the feature in the form of quartz (53.87%), calcite (34.56%), kaolinite (6.54%), and illite minerals (5.04%). The minor presence of kaolinite and illite minerals might represent epithermal and argillic alteration, as these minerals would only form at relatively low temperature. Hydrothermal alteration on the feature might result from the drawing down of surficial waters through the two dextral strike-slip faults in the middle of the Gapuro Sagoro Seamount, which might explain the formation of the Yudo Sagoro Hill. Based on this interpretation, the second model (Fig. 5b) represents the most probably subsurface structure beneath Yudo Sagoro Hill as the model consists of two bodies with different susceptibilities. The two bodies indicate the presence of either alteration of volcanic material or serpentinisation of exposed peridotite. Both processes could be triggered by the interaction between the seawater and the wall rock. Therefore, the source of magnetisation over the feature other than from fresh volcanic structure is still open for further investigation, whether it comes from altered volcanic materials or from serpentinised peridotite. One caveat of our interpretation would be the limited clay and silt samples obtained from the top of the feature, which was not more than 6.04 g. Further studies involving seafloor sampling at several sampling stations on the Yudo Sagoro Hill will enrich our understanding of the subsurface structure of the feature and the history of its hydrothermal activities.

### Acknowledgements

The authors would like to thank the Chief of Staff of the Indonesian Navy and the Committee for the 100th Anniversary Celebration Committee of Hydrographic Sciences for initiating the Jalacitra I-2021 expedition 'Aurora'. We would also like to thank the Commander and the crew of KRI Spica 934, who have carried out the survey with the utmost dedication, and all participating scientists for their invaluable contribution to the onboard discussions. Licensed software is made available by the Indonesian Hydro-Oceanographic Centre (Pushidrosal). Transformations from total magnetic intensity to magnetic anomalies processes were carried out in Matlab R2021a, employing script packages of M. Tivey, Woods Hole Oceanographic Institute (WHOI). The script packages were previously stored on the website [deeptow.whoi.edu/download.html](http://deeptow.whoi.edu/download.html). Access to the script packages at the moment should be available through personal contact. The authors profoundly recognise the constructive review from R. Hall and an anonymous reviewer to the manuscript.

### Author contributions

GA initiated the regional tectonic studies, designed, processed, and interpreted the magnetic anomaly, carried out the 2.5-D magnetic modelling,

interpreted the multibeam bathymetry, led the writing of the manuscript, and secured publication funding. N and DPS are instrumental in the conceptualisation of the project, the acquisition of research funding, the administration of the project, and overall project supervision. DA designed, carried out, processed, and reported the sediment and seafloor sampling processes. AD and SS designed, processed, and interpreted the multibeam backscatter data, observed the seafloor sampling processes, and described the obtained seafloor biota. MH and AP supervised the regional tectonic studies and provided regional geophysical and geological references to aid in interpretation. IAK carried out the XRD test and interpretation. P supervised the general reporting and writing processes and supported the acquisition of publication funding. CMG supervised the 2.5D magnetic modelling and interpretation. AMM supervised the treatment of the seafloor sample obtained and the interpretation of the discovered feature. All authors discussed the results and contributed to various parts of the manuscript.

### Funding

This research is funded by the Indonesian Navy through the “100th Anniversary of Hydrographic Sciences Celebration” in 2021, organised by the Hydro-Oceanographic Centre (Pushidrosal), Indonesian Navy. The publication of this research is funded by World-Class University funding of the Institute of Research and Community Service (LPPM), Institut Teknologi Bandung, Indonesia (2022/2023).

### Data availability

Access to each data set can be made available by request to pusdalops@pushidrosal.id.

### Code availability

Not applicable.

### Declarations

### Competing interests

The authors declare no competing interest.

Received: 6 April 2023 Accepted: 4 October 2023

Published online: 13 October 2023

### References

- Aina A (1986) Reduction to equator, reduction to pole and orthogonal reduction of magnetic profiles. *Explor Geophys* 17(3):141–145
- Alken P, Thébaud E, Beggan CD, Amit H, Aubert J, Baerenzung J, Bondar TN, Brown WJ, Califf S, Chambodut A, Chulliat A, Cox GA, Finlay CC, Fournier A, Gillet N, Grayver A, Hammer MD, Holschneider M, Huder L, Hulot G, Jager T, Kloss C, Korte M, Kuang W, Kuvshinov A, Langlais B, Léger J-M, Lesur V, Livermore PW, Lowes FJ, Macmillan S, Magnes W, Mandea M, Marsal S, Matzka J, Metman MC, Minami T, Morschhauser A, Mound JE, Nair M, Nakano S, Olsen N, Pavón-Carrasco FJ, Petrov VG, Ropp G, Rother M, Sabaka TJ, Sanchez S, Saturnino D, Schnepf NR, Shen X, Stolle C, Tangborn A, Tøffner-Clausen L, Toh H, Torta JM, Varner J, Vervelidou F, Vigneron P, Wardinski I, Wicht J, Woods A, Yang Y, Zeren Z, Zhou B (2021) International Geomagnetic Reference Field: the thirteenth generation. *Earth Planets Space* 73(1):49
- Ballantyne P (1991) Petrological constraints upon the provenance and genesis of the East Halmahera ophiolite. *J Southeast Asian Earth Sci* 6(3–4):259–269
- Ballantyne P (1992) Petrology and geochemistry of the plutonic rocks of the Halmahera ophiolite, eastern Indonesia, an analogue of modern oceanic forearcs. *Geol Soc London Spec Publ* 60(1):179–202
- Bloomer SH (1983) Distribution and origin of igneous rocks from the landward slopes of the Mariana Trench: Implications for its structure and evolution. *J Geophys Res Solid Earth* 88(B9):7411–7428
- Breiner S (1973) Applications manual for portable magnetometers, vol 395. Geometrics, Sunnyvale
- Cardwell RK, Isaacks BL, Karig DE (1980) The spatial distribution of earthquakes, focal mechanism solutions, and subducted lithosphere in the Philippine and northeastern Indonesian islands. *Wash. DC Am. Geophys Union Geophys Monogr Ser* 23:1–35
- Castro FR, Oliveira SP, De Souza J, Ferreira FJF (2018) Grav-Mag Suite: an open source MATLAB-based program for processing potential field data. *VIII Simp Bras Geofis.* 8:1
- Charlton TR, Hall R, Partoyo E (1991) The geology and tectonic evolution of Waigeo Island, NE Indonesia. *J Southeast Asian Earth Sci* 6(3–4):289–297
- Chen YJ (1992) Oceanic crustal thickness versus spreading rate. *Geophys Res Lett* 19(8):753–756
- Cooper GRJ (1998) GEOMODEL for Windows 2.5-D interactive magnetic and gravity data modelling and inversion.
- Corbett GJ, Leach T (1997) Short course manual. Southwest Pacific rim gold-copper syst.: Structure, alteration and mineralization, 5, 97.
- Corbett GJ (2008) Influence of Magmatic Arc Geothermal Systems on Porphyry–Epithermal Au–Cu–Ag Exploration Models. In Terry Leach Symp., Sydney (Vol. 17).
- Di Giacomo D, Engdahl ER, Storchak DA (2018) The ISC-GEM earthquake catalogue (1904–2014): status after the extension project. *Earth Syst Sci Data* 10(4):1877–1899
- Dietze F, Kontny A, Heyde I, Vahle C (2011) Magnetic anomalies and rock magnetism of basalts from Reykjanes (SW-Iceland). *Studia Geophys Geodaetica* 55(1):109–130
- Dimalanta CB, Faustino-Eslava DV, Gabo-Ratio JAS, Marquez EJ, Padrones JT, Payot BD, Queano KL, Ramos NT, Yumul GP Jr (2020) Characterization of the proto-Philippine Sea Plate: evidence from the emplaced oceanic lithospheric fragments along eastern Philippines. *Geosci Front* 11(1):3–21
- Eikström G, Nettles M, Dziewoński AM (2012) The global CMT project 2004–2010: Centroid-moment tensors for 13,017 earthquakes. *Phys Earth Planet Inter* 200:1–9
- Fonseca L, Calder B (2005) Geocoder: an efficient backscatter map constructor. In: Proceedings of the US hydrographic. San Diego, CA
- Fonseca L, Mayer L (2007) Remote estimation of surficial seafloor properties through the application angular range analysis to multibeam sonar data. *Mar Geophys Res* 28(2):119–126
- Fonseca L, Brown C, Calder B, Rzhavov Y (2009) Angular range analysis of acoustic themes from Stanton Banks Ireland: a link between visual interpretation and multibeam echosounder angular signatures. *Appl Acoust* 70(10):1298–1304
- Fryer P (1996) Evolution of the Mariana convergent plate margin system. *Rev Geophys* 34(1):89–125
- Fryer P (2012) Serpentinite mud volcanism: observations, processes, and implications. *Annu Rev Mar Sci* 4:345–373
- Fujiwara T, Tamaki K, Fujimoto H, Ishii T, Seama N, Toh H, Koizumi K, Igarashi C, Segawa J, Kobayashi K, Kido M (1995) Morphological studies of the Ayu trough, Philippine sea–Caroline plate boundary. *Geophys Res Lett* 22(2):109–112
- GEBCO Bathymetric Compilation Group 2022, 2022. The GEBCO\_2022 Grid – a continuous terrain model of the global oceans and land. *NERC EDS Br. Oceanogr. Data Cent. NOC.*
- Hall R (1987) Plate boundary evolution in the Halmahera region. *Indonesia Tectonophysics* 144(4):337–352
- Hall R (2002) Cenozoic geological and plate tectonic evolution of SE Asia and the SW Pacific: computer-based reconstructions, model and animations. *J Asian Earth Sci* 20(4):353–431
- Hall R, Audley-Charles MG, Banner FT, Hidayat S, Tobing SL (1988a) Basement rocks of the Halmahera region, eastern Indonesia: a Late Cretaceous–Early Tertiary arc and fore-arc. *J Geol Soc* 145(1):65–84
- Hall R, Audley-Charles MG, Banner FT, Hidayat S, Tobing SL (1988b) Late Palaeogene–Quaternary geology of Halmahera, Eastern Indonesia: initiation of a volcanic island arc. *J Geol Soc* 145(4):577–590
- Hall R, Ali JR, Anderson CD (1995a) Cenozoic motion of the Philippine Sea Plate: palaeomagnetic evidence from eastern Indonesia. *Tectonics* 14(5):1117–1132
- Hall R, Fuller M, Ali JR, Anderson CD (1995b) The Philippine sea plate: magnetism and reconstructions. *Active Margins Margin Basins Western Pacific.* 88:371–404
- Hamilton WB (1979). *Tectonics of the Indonesian region* (Vol. 1078). US Government Printing Office.

- Hutchison C (1986) Formation of marginal seas in Southeast Asia by rifting of the Chinese and Australian continental margins and implications for the Borneo region. *Buletin-Persatuan Geol Malays* 20:201–220
- Kloser R, Keith G (2013) Seabed multi-beam back scatter mapping of the Australian continental margin. *Acoust Aust* 41(1):65–72
- Lawless JV, Bromley CJ, Leach TM, Licup Jr, AC, Cope DM, Recio CM (1983) Bacon-Manito geothermal field: a geoscientific exploration model. In *New Zealand geothermal workshop*. 5 (pp. 97–102)
- Leach TM, Umali DU, Del Rosario RC, (1985) Epithermal mineral zonation in an active island arc: the Bacon-Manito geothermal systems, Philippines. In *New Zealand geothermal workshop*. 7 (pp. 109–114).
- Lee SM, Kim SS (2004) Vector magnetic analysis within the southern Ayu Trough, equatorial western Pacific. *Geophys J Int* 156(2):213–221
- Lutz RA, Kennish MJ (1993) Ecology of deep-sea hydrothermal vent communities: a review. *Rev Geophys* 31(3):211–242
- McCaffrey R (1982) Lithospheric deformation within the Molucca Sea arc-arc collision: evidence from shallow and intermediate earthquake activity. *J Geophys Res* 87(B5):3663–3678
- Milsom J, Masson D, Nichols G, Sikumbang N, Dwiyanto B, Parson L, Kallagher H (1992) The Manokwari trough and the western end of the New Guinea trench. *Tecton* 11(1):145–153
- Milsom J, Hall R, Padmawidjaja T (1996a) Gravity fields in eastern Halmahera and the Bonin Arc: implications for ophiolite origin and emplacement. *Tecton* 15(1):84–93
- Milsom J, Parson L, Masson D, Nichols G, Sikumbang N, Dwiyanto B (1996b) Tectonics of the Palau-Halmahera-Waigeo Triangle
- Mutter CZ, Mutter JC (1993) Variations in thickness of layer 3 dominate oceanic crustal structure. *Earth Planet Sci Lett* 117(1–2):295–317
- Nabighian MN (1972) The analytic signal of two-dimensional magnetic bodies with polygonal cross-section: its properties and use for automated anomaly interpretation. *Geophys* 37(3):507–517
- Nichols G, Hall R, Milsom J, Masson D, Parson L, Sikumbang N, Dwiyanto B, Kallagher H (1990) The southern termination of the Philippine Trench. *Tectonophysics* 183(1–4):289–303
- Noutchogwe CT, Koumetio F, Manguelle-Dicoum E (2010) Structural features of South-Adamawa (Cameroon) inferred from magnetic anomalies: Hydrogeological implications. *Comptes Rendus Geosci* 342(6):467–474
- Oufi O, Cannat M, Horen H (2002) Magnetic properties of variably serpentinized abyssal peridotites. *J Geophys Res* 107(B5):3
- Prezzi C, Orgeira MJ, Ostera H, Vasquez CA (2005) Ground magnetic survey of a municipal solid waste landfill: pilot study in Argentina. *Environ Geol* 47(7):889–897
- Pushidrosal (1955) *Berita Pelaut Indonesia* (BPI) no. 11/152. In: *Berita Pelaut Indonesia* no. 01 – 26 – 1955. Jakarta: Pushidrosal, pp 11
- Pushidrosal (1959) *Berita Pelaut Indonesia* (BPI) no. 26/206. In: *Berita Pelaut Indonesia* no. 01 – 26 – 1959. Jakarta: Pushidrosal, pp.2
- Pushidrosal (2022) *Indonesia Undersea Features Name: Halmahera and Banda Sea*. In: 35<sup>th</sup> GEBCO Sub-Comm. Undersea Feature Names (SCUFN) Meet. 2002
- Reyes A (1991) Mineralogy, distribution and origin of acid alteration in Philippine geothermal systems. *Chishitsu Chosajo Hokoku* (Report, Geol. Surv. Japan); (Japan), 277.
- Salem A, Ravat D, Gamey TJ, Ushijima K (2002) Analytic signal approach and its applicability in environmental magnetic investigations. *J Appl Geophys* 49(4):231–244
- Sandwell DT, Müller RD, Smith WH, Garcia E, Francis R (2014) New global marine gravity model from CryoSat-2 and Jason-1 reveals buried tectonic structure. *Sci* 346(6205):65–67
- Schneider J, De Wall H, Kontny A, Bechstädt T (2004) Magnetic susceptibility variations in carbonates of the La Vid Group (Cantabrian Zone, NW-Spain) related to burial diagenesis. *Sediment Geol* 166(1–2):73–88
- Simmons SF, Christensen BW (1994) Origins of calcite in the Broadlands-Ohaaki geothermal system, New Zealand. *Am J Sci* 294:361–400
- Smith W, McIntyre AD (1954) A spring-loaded bottom-sampler. *J Mar Biol Assoc U K* 33(1):257–264
- Su W, Mutter CZ, Mutter JC, Buck WR (1994) Some theoretical predictions on the relationships among spreading rate, mantle temperature, and crustal thickness. *J Geophys Res* 99(B2):3215–3227
- Swain CJ (2000) Reduction-to-the-pole of regional magnetic data with variable field direction, and its stabilisation at low inclinations. *Explor Geophys* 31(2):78–83
- Taran Y, Kalacheva E (2020) Acid sulfate-chloride volcanic waters; Formation and potential for monitoring of volcanic activity. *J Volcanol and Geotherm Res* 405:107036
- Veikkolainen T, Korhonen K, Pesonen LJ (2014) On the Spatial Averaging of Paleomagnetic Data. *Geophys.s* 50(1).
- Wakabayashi J, Ghatak A, Basu AR (2010) Suprasubduction-zone ophiolite generation, emplacement, and initiation of subduction: a perspective from geochemistry, metamorphism, geochronology, and regional geology. *Bull* 122(9–10):1548–1568
- Waters KE, Rowson NA, Greenwood RW, Williams AJ (2007) Characterising the effect of microwave radiation on the magnetic properties of pyrite. *Sep Purif Technol* 56(1):9–17
- Weissel JK, Anderson RN (1978) Is there a Caroline plate? *Earth Planet Sci Lett* 41(2):143–158
- Wessel P, Smith WH, Scharroo R, Luis J, Wobbe F (2013) Generic mapping tools: improved version released. *Eos Trans Am Geophys Union* 94(45):409–410.
- Wheat CG, Seewald JS, Takai K (2020) Fluid transport and reaction processes within a serpentinite mud volcano: South Chamorro Seamount. *Geochim Cosmochim Acta* 269:413–428
- Wienberg C, Bartholomä A (2005) Acoustic seabed classification in a coastal environment (outer Weser Estuary, German Bight)—a new approach to monitor dredging and dredge spoil disposal. *Cont Shelf Res* 25(9):1143–1156

## Publisher's Note

Springer Nature remains neutral with regard to jurisdictional claims in published maps and institutional affiliations.

Submit your manuscript to a SpringerOpen<sup>®</sup> journal and benefit from:

- Convenient online submission
- Rigorous peer review
- Open access: articles freely available online
- High visibility within the field
- Retaining the copyright to your article

Submit your next manuscript at ► [springeropen.com](https://www.springeropen.com)